Reaction mechanism of aluminum nanoparticle: atomic-level physicochemical reaction and heat/mass transfer

Qingzhao Chu[1], Baolu Shi[1]*, Lijuan Liao[2]*, Xiangrui Zou[1], Kai.H Luo[3], Ningfei, Wang[1]

[1] School of Aerospace Engineering, Beijing Institute of Technology, No.5 ZhongGuanCun South Street, Haidian, Beijing, 100081, CHINA

[2] Key Laboratory for Mechanics in Fluid Solid Coupling Systems, Institute of Mechanics, Chinese Academy of Sciences, No. 15 BeiSihuan West Road, Beijing, 100190, CHINA

[3] Department of Mechanical Engineering, University College London, Torrington Place, London WC1E 7JE, United Kingdom

Corresponding Authors:

Baolu Shi [1*]   E-mail: shibaolu@bit.edu.cn, smashingsky@hotmail.com

Tel: +86-10-6891-3623

School of Aerospace Engineering, Beijing Institute of Technology, No.5 ZhongGuanCun South Street, Haidian, Beijing, 100081, CHINA

Lijuan Liao[2**]   Email: liaohuanxin@hotmail.com   Tel: +86-10-8254-4291.

Institute of Mechanics, Chinese Academy of Sciences, No. 15 BeiSihuan West Road, Beijing, 100190, CHINA

Highlights

- ANP reaction experiences physical and chemical adsorption as well as condensed diffusion

- Al-oxidizer atom binding energy determines ANP microstructure via oxidant diffusion

- Reaction with high Al binding energy shows high heat release but weak mass diffusivity

- Melting and ignition temperatures vary slightly with oxidizer types and H_2O/CO_2 atmospheres accelerate preheating

Graphic Abstract
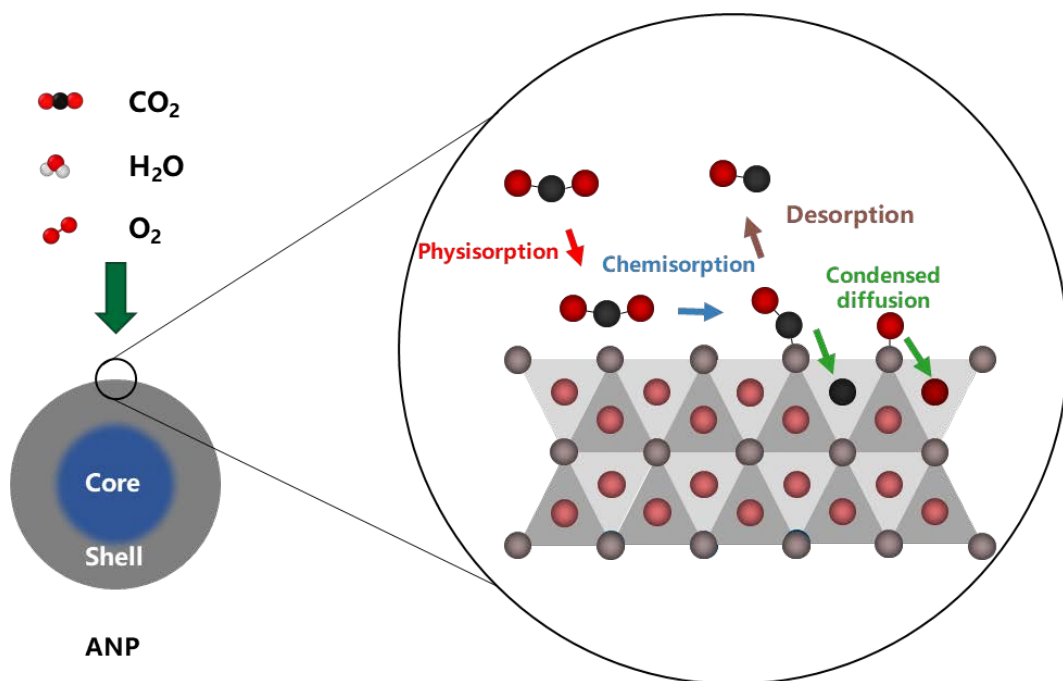
Abstract

To capture core-shell Al/Al_2O_3 nanoparticle (ANP) reaction mechanisms in different oxidizers, this study examined the detailed physicochemical process for ANP burning in high temperature CO_2, H_2O and O_2 environments at the atomic-level. The evolutions of oxidizer-particle reaction, particle structure, environmental species, heat transfer and reaction heat release were investigated. Three kinds of interactions, including physical adsorption, chemical adsorption and condensed diffusion were observed. The results show that initially oxidizer molecules are physically and chemically adsorbed on the ANP surface to prompt ANP melting through heat transfer and surface reaction. Before ignition the oxidizer molecules remain on the ANP surface, thereafter some of the surface adsorbed oxidizer atoms diffuse across the shell and react with the Al core. With low adsorption energy, H_2O molecules show remarkable physical adsorption before core melting, while chemical adsorption plays an important role in high-adsorption-energy oxidizers like CO_2 and O_2. The binding energy between the ANP and oxidizer atoms directly influences condensed diffusion, leading to different ANP structures as well as heat release rates. Since most of the adsorbed oxidizer atoms remain on the surface before ignition, the temperatures for core Al melting and ANP ignition are almost the same in different oxidizers.

Keywords: Physicochemical adsorption, surface reaction, condensed diffusion, heat transfer, microstructure evolution

1. Introduction

Due to their high specific energy density (31 kJ/g) and abundance on earth, aluminum particles have been widely used as energetic materials in many combustion and explosive systems, such as space propulsion [1], underwater propulsion [2], and even gas turbine engines [3]. Conventional low-cost Al powders are composed of particles on the scale of tens of micrometers or larger in size. Ignition difficulties of Al particles occur as a result of the alumina oxide shell, which separates the reactive Al core from oxidizer gases. Additional problems include incomplete combustion caused by large particles and agglomerates along with deposition of condensed products on nozzles [4]. To meet these challenges, aluminum nanoparticle (ANP) has been proposed as an alternative to its micron-sized counterpart. With high surface to volume ratio and short diffusion distance, ANP has excellent physicochemical properties, such as low ignition temperature and high reaction rates [5].

In ANP combustion, the oxidizer plays a significant role. ANP-O_2 combustion has been widely investigated due to O_2 richness in air [6–9]. However, in some practical applications, the environment contains little oxygen. In solid rocket engines, for example, ANP reacts with propellant products that mainly consist of CO_2 and H_2O. In Mars space exploration missions, where the planet's atmosphere mainly consists of CO_2, combustion of ANP in CO_2 may supply the main energy for propulsion [10]. Besides, H_2O is the primary oxidizer for under-water propulsion. Thus, it is indispensable to

understand the mechanisms of ANP reaction in CO_2, H_2O and O_2 atmospheres.

Over the past decades, considerable efforts have been made to study the reaction mechanism of ANP, which is strongly affected by particle size [11], oxidizer property [12], environmental temperature and pressure [13,14]. The ignition and combustion characteristics were investigated by Yang et. al. [15]. Based on experimental results, they proposed a theoretical model that divides the ignition and combustion process into several stages. As the temperature increases, the oxide layer fractures and the aluminum flows outward, and then surface heterogeneous reaction takes place. Before ignition, the heating of ANP is mainly attributed to conduction and radiation heat transfer [15]. When considering the combustion characteristics of ANP in gaseous oxidizers, the effective oxidizer mole fraction is widely adopted [16], which is defined as $X_{eff} = X_{O2} + 0.6X_{H2O} + 0.22X_{CO2}$, where X is the mole fraction of the oxidizing chemical species for the aluminum particle. These studies have shed some light on the complexity, but the understanding is far from being complete. The difficulty of studying ANP ignition and combustion lies in the evolution of microstructure and gas-particle interaction under extremely small time and length scales.

Recently, the Reactive Molecular Dynamics simulation has been employed to study oxidation of ANP [17–20]. However, most of these works focus on combustion characteristics of ANP with oxygen after ignition. In our previous work [21], four different stages were defined for ANP burning in O_2, and the effects of ambient

temperature and pressure on each stage were discussed. The atomic diffusion inside ANP was also examined to depict the evolution of the ANP structure in a high temperature oxygen atmosphere. However, several key questions remain unanswered, including the detailed physical and chemical interactions between ANP and typical oxidizers during the reaction process, as well as the corresponding heat transfer and chemical heat release characteristics.

This study aims to obtain an insightful understanding of the detailed physicochemical process of core-shell ANP combustion and examine the essential differences in the reaction and heat transfer mechanisms of ANP burning in CO_2, H_2O and O_2 environments, respectively. A core-shell ANP with temperature of 300 K is put into a high temperature (2000 K) CO_2 environment, and the detailed reaction process between ANP and CO_2 is firstly investigated. Then the contributions of heat transfer and reaction to the ANP melting and ignition are discussed. Thereafter, the reactions of ANP/H_2O and ANP/O_2 combinations are examined and compared to reveal the ANP reaction mechanisms.

2. Methodology

The reactive force field (ReaxFF) molecular dynamics (MD) was adopted to simulate the reaction of ANP with CO_2/H_2O/O_2. The Al/C/H/O ReaxFF parameters used in this paper have been trained and validated by Hong et al. [22,23] , which have

been applied in oxidation of Al/O_2 [24–26], Al/ethanol [18], Al/graphene oxide [27] and Al/ether [28] systems.

The core-shell ANP was prepared following the method introduced in our previous study, which consisted of an Al core with a 2 nm radius and an oxide shell with a 2 nm thickness. Detailed information can be found in Ref. [21]. Then, the prepared ANP was put into an environment consisting of 2700 oxidizer molecules with a temperature of 2000 K in a box of 160 Å×160 Å×160 Å. Three typical oxidizers CO_2, H_2O and O_2 were selected. The system was then simulated under the NVE ensemble for 160 ps to examine the reaction of the ANP. A time step of 0.2 fs was used for time integration, which has proved to be able to capture ANP oxidation behaviors while keeping computational cost low [21]. Periodic boundary conditions were implemented in all three directions. At least three samples were performed for each case to obtain a reliable result. ReaxFF MD simulations were conducted with the LAMMPS package [29]. OVITO was used to visualize atomic configurations [30].

To react with ANP, oxidizer molecules should firstly contact ANP at its surface. Hence, to make quantitative analysis, it is indispensable to define the position of the ANP surface. In this study, the ANP is divided into many shells with very small bin size, and the number of Al atoms in each shell can be calculated against the particle radius (R), as plotted in Fig. 1. The radius of the ANP surface (R_s) is defined as the radius of a shell where the Al atom number is half of the maximum value (Fig. 1a). Here, different bin sizes from 0.1 to 1 Å have been tested (Fig. 1b). It is found that the bin size of 0.5

Å is able to accurately capture the representative ANP surface. Accordingly, the surface region is defined as the shell within $R_s \pm \delta$ (light blue region lying between two dashed curve circles in Fig. 1c). Since the chemical bond length of Al-C, H, O is shorter than 2 Å, different values of δ ranging from 1.6 to 2 Å have also been tested. The sensitivities of δ has been discussed in terms of the temporal variations of surface atom number density in Supporting Information (Fig. S1). A value of $\delta = 1.8$ Å is sufficient to obtain reasonable results in three oxidizers.
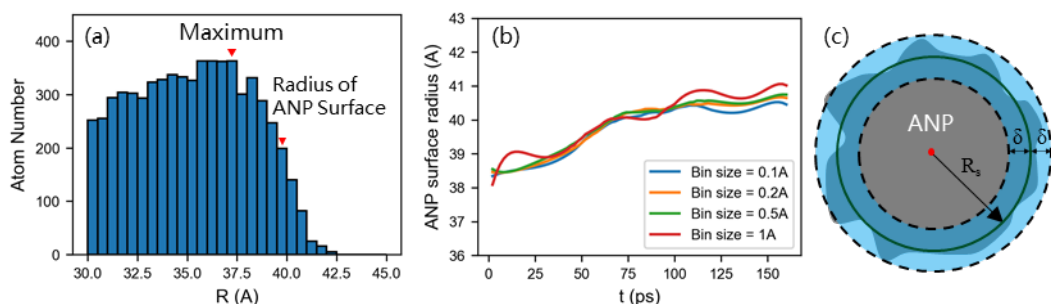

Figure 1 (a) Number of Al atoms in the shells towards outer surface, (b) temporal variation of ANP surface radius with bin sizes 0.1-1 Å, and (c) illustration of ANP surface region.

3. Results and discussion

By performing ReaxFF MD, Section 3.1 presents the characteristics of ANP reaction in CO_2, including collision process by atom trajectories, variation of oxidizer and adsorbed atoms, evolution of the ANP structure, and the contribution of heat transfer and reaction. Then Section 3.2 presents the results and discussion of the ANP/H_2O and ANP/O_2 systems; and by summarizing their similarities and differences, conclusions are drawn in Secion 4.

3.1 Characteristics of ANP-CO$_2$ reaction

3.1.1 Interaction between ANP and CO$_2$

In the reaction process, environmental oxidizer molecules firstly become adsorbed on the ANP surface through collisions. Then some of the oxidizer atoms may diffuse into the core across the ANP surface. To investigate the collision dynamics between ANP and gaseous oxidizer molecules, the trajectories of 2700 CO$_2$ molecules were analyzed. According to their behaviors after collision, three representative trajectories are summarized, as illustrated in Fig. 2.
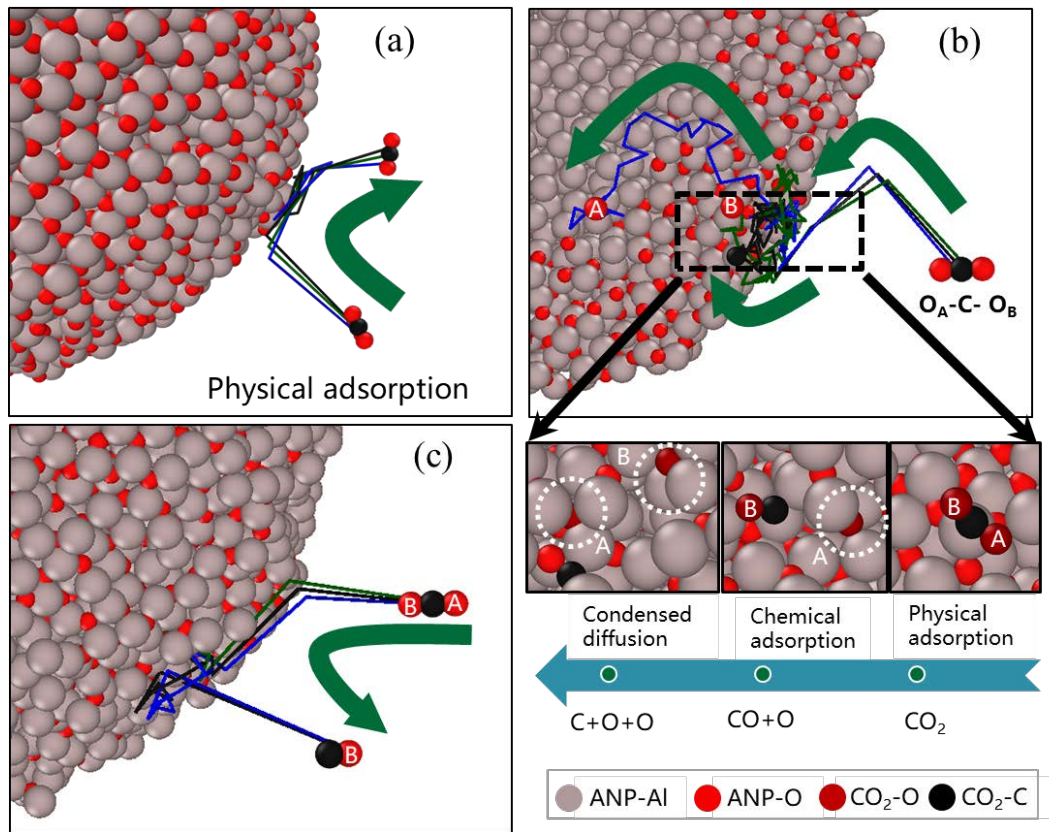

Figure 2 Trajectories of collision between ANP and CO$_2$ molecules: (a) physical adsorption and desorption of CO$_2$, (b) physical and chemical adsorption as well as

condensed diffusion, and (c) physical and chemical adsorption of CO_2 and CO desorption.

In Fig. 2a, initially a representative CO_2 molecule gradually moves toward the ANP surface, and gets adsorbed on the surface; after staying for a short while, it escapes the ANP surface, as the bold arrow illustrates. This trajectory indicates that there is no bond break or formation for the CO_2 molecule. This process is mainly induced by the van der Walls force without bond break, which is defined as physical adsorption.

In Fig. 2b, a representative CO_2 molecule (marked as O_A-C-O_B) is firstly adsorbed and stays on the ANP surface (see enlarged snapshots at the bottom); thereafter, one C-O bond of the CO_2 molecule breaks and an O atom (O_A) diffuses into the ANP, leaving a CO molecule (C-O_B) on the surface. Then, C-O_B bond of the CO molecule also breaks and the oxygen atom (O_B) diffuses inward. During the processes, the oxidizer molecule's bond breaks and the detached atom is adsorbed at the ANP surface, which is defined as chemical adsorption here; then theses adsorbed atoms diffuse across shells to form new bonds inside the ANP, which is defined as condensed diffusion. This definition is similar to that in ref. [31], as a diffusion process whereby the random thermally-activated movement of atoms in a solid or liquid phase, resulting in the directed transport of atoms.

It is interesting to note that not all adsorbed oxidizer atoms may totally diffuse into the oxide shell. Some of them remain on the ANP surface and desorb to form new gas

molecules, as illustrated in Fig. 2c, in which CO desorption is observed. In the latter section, we will explain this phenomenon from the perspective of adsorption energy.

Accordingly, the ANP-oxidizer interaction can be classified into three kinds from the perspective of bond break and formation: physisorption, chemisorption and condensed diffusion. In DFT simulation, adsorption energy and bond length are usually adopted as the criteria to differentiate physical adsorption from chemical adsorption for unimolecular adsorption reaction [32,33]. While in multi-molecular adsorption cases, it is difficult to detect the adsorption energy of each single molecule due to disturbance of other adsorbates. In this study, bond length is selected to differentiate adsorption state.

To determine the critical bond length, a α-Al_2O_3 (001) slab is used to analogize the ANP surface. The physically adsorbed structure of the oxidizer molecule on the slab is minimized to obtain stable bond length. In ANP/CO_2 adsorption, because C atom in CO_2 is more favorable to adsorb on Al atom at the ANP surface, the Al-C bond length is used to represent the degree of adsorption. Similarly, in ANP/H_2O and ANP/O_2 systems, the Al-O bond between ANP and oxidizer is used. The stable bond lengths for physical (L_{phy}) adsorptions are listed in Table 1. When the oxidizer breaks intramolecular bond and turns to chemical adsorption state, its bond with the ANP surface becomes shorter. To distinguish physical/chemical adsorption states, the adsorption with bond length shorter than L_{phy} is considered as chemical adsorption state. Corresponding adsorption energies are also listed in Table 1. The adsorption energy is

defined as $E_{\text{adsorption}} = E_{\text{surface+sorbent}} - (E_{\text{surface}} + E_{\text{sorbent}})$, where $E_{\text{surface+sorbent}}$, E_{surface} and E_{sorbent} are the energy of the surface with the adsorbed molecule, the surface and the gas molecule, respectively. During condensed diffusion, the oxidizer atoms diffuse into ANP. The number of oxidizer atoms of condensed diffusion is determined by their radial position. If their radial position is less than the inner boundary of the surface region (R_s-δ), these atoms are considered to be in condensed diffusion state.

Table 1 Stable bond lengths and adsorption energy of physical adsorption.

System	Bond type	L_{phy} (A)	E_{ad} (kcal/mol)
ANP/CO_2	Al-C	2.03	-102.11
ANP/H_2O	Al-O	2.189	-67.55
ANP/O_2	Al-O	1.85	-94.43

To further investigate details of the surface interaction, the temporal evolutions of ambient species in the environment are computed and plotted in Fig. 3a. In this study, the solid lines are the average of three runs, whereas the translucent area indicates the error band. To demonstrate representative time instants during the whole reaction, the boundaries for the four stages of preheating, Al core melting, fast core oxidation and shell oxidation are also illustrated by the dash, dash-dot and dot lines, respectively [21]. In Fig. 3a, there are mainly two gas species (CO_2 and CO) during reaction. The sum of

other species, like O, O_2 and C, is less than 2. CO_2 and CO molecules are continuously consumed due to adsorption, and the consuming rate increases after ignition (indicated by the dash-dot line). Around t = 90 ps, CO molecules appear in the environment, and their number gradually increases.
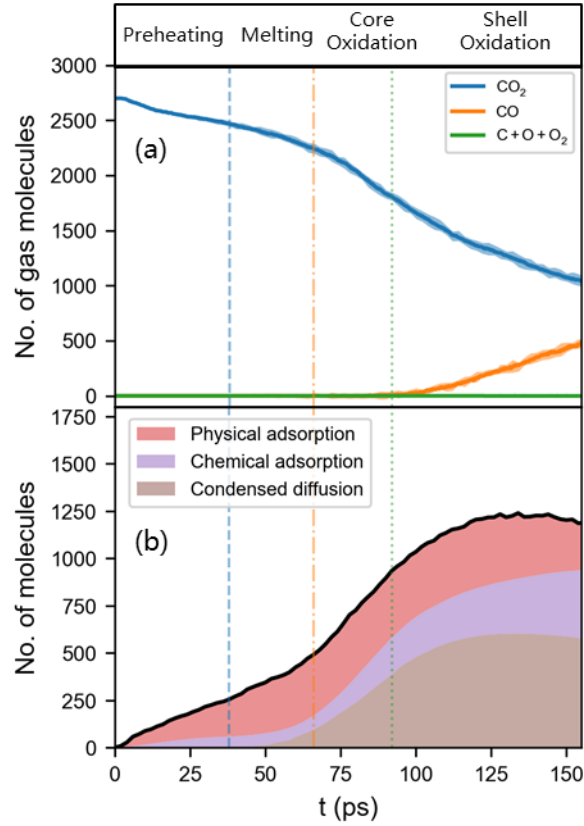

Figure 3 Evolution of numbers of molecules or atoms in the ambient (a) and computed number of oxidizer molecules in physical, chemical adsorption and condensed diffusion state (b). The dash, dash-dot and dot lines represent the end of preheating, melting, fast core oxidation stages [21], respectively.

To quantitively analyze the dynamics of physical/chemical adsorption and

condensed diffusion, carbon atom in CO_2 is adopted to track the migration of the oxidizer molecules. As plotted in Fig. 3b, the physisorption (red contour) dominates during the preheating stage, and chemisorption accompanies physical adsorption with a relatively low proportion; in melting stage, the number of molecules in chemisorption gradually increases, while the number of physically adsorbed molecules remains unchanged. For chemical adsorption, bond breaking needs activated energy. Before ignition, the ANP temperature is relatively low (less than 1600 K), leading to rare chemically adsorbed oxidizer molecules on the ANP surface. Meanwhile, chemical adsorption is the precondition before condensed diffusion, thus the number of molecules condensed diffusion is rarer before ignition. After ignition, chemical adsorption as well as condensed diffusion becomes increasingly remarkable. Near 125 ps, the number of totally adsorbed molecules reaches a plateau, although CO_2 molecules keep a high consuming rate.

The oxidizer adsorption and condensed diffusion directly influence ANP reaction, determining the evolution of the ANP microstructure. Here the radial distributions of the atom number density at typical stages of initial, near ignition, core runout and end of simulation are investigated to track the diffusion of different atoms. A slice snapshot (refer to Fig. 4e) is also provided at the bottom in Fig. 4a-d. Comparing the number density plots at the initial state and near ignition, it is found that the density of core decreases due to core melting and ANP expansion. Oxygen atoms in the oxide shell gradually diffuse into the core, leaving tiny vacant sites in the oxide shell. The number

14

density of adsorbed oxidizer atoms is low and most of the adsorbed atoms remain on the ANP surface (Fig. 4b). After ignition, plenty of shell O atoms diffuse into the core, leading to shrinking Al core. Meanwhile, the diffusion of adsorbed oxidizer atoms enhances, resulting in increase in O and C number densities, as shown in Fig. 4c. At the end of simulation, Al and O atoms distribute uniformly. The number density of adsorbed C atoms shows a slight increase, and these atoms distribute on the ANP surface, indicating relatively low diffusivity, even though the overall number of condensed diffusion C atoms increases much, as illustrated in Fig. 4e.
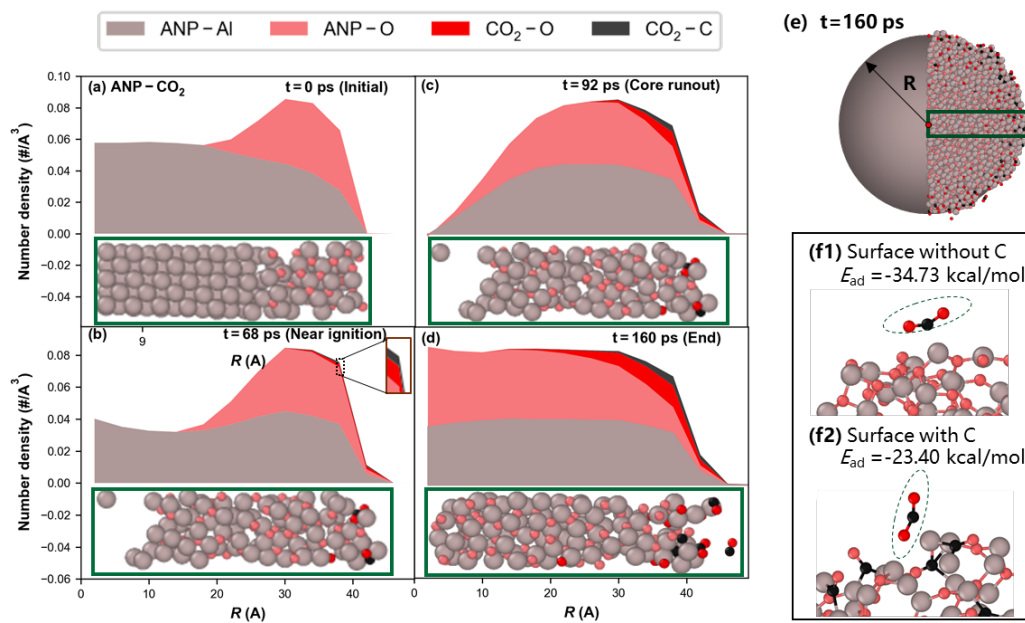

Figure 4 Radial number density distribution (top) and slice snapshot (bottom) of ANP at initial state (a), near ignition (b), core runout (c) and simulation end (d), illustration of C atoms distribution, and adsorption energy of CO_2 molecule on different surfaces (f).

Furthermore, in Fig. 4d, CO moleculars are observed in the environment. This may

be attributed to the variation of the ANP surface structure after C atoms adsorption, which might alter the potential energy surface of ANP. Here the effect of surface C atom coverage on CO_2 adsorption is investigated by the adsorption energy of the ANP surface with different C concentrations. Two typical cases, surface without C and with a relatively high C number density, are tested, as illustrated in Fig. f1-2. The surface without any C atom is the raw amorphous alumina surface at 0 ps, while the surface with C atoms is cutting from the ANP at t = 100 ps, where there have already been C atoms bonded to the surface Al atom. On the raw surface without any C atom, CO_2 molecules are adsorbed on Al sites with C atom toward surface Al atom. As the surface C atom concentration increases (Fig. f2), the adsorption energy decreases, indicating that CO_2 adsorption stability on the ANP surface is impeded by increased surface C atom concentration. Meanwhile, the O atom of CO_2 is close to Al of ANP. Thus, CO_2 dissociation tends to produce CO molecule and leave O atom on the ANP surface.
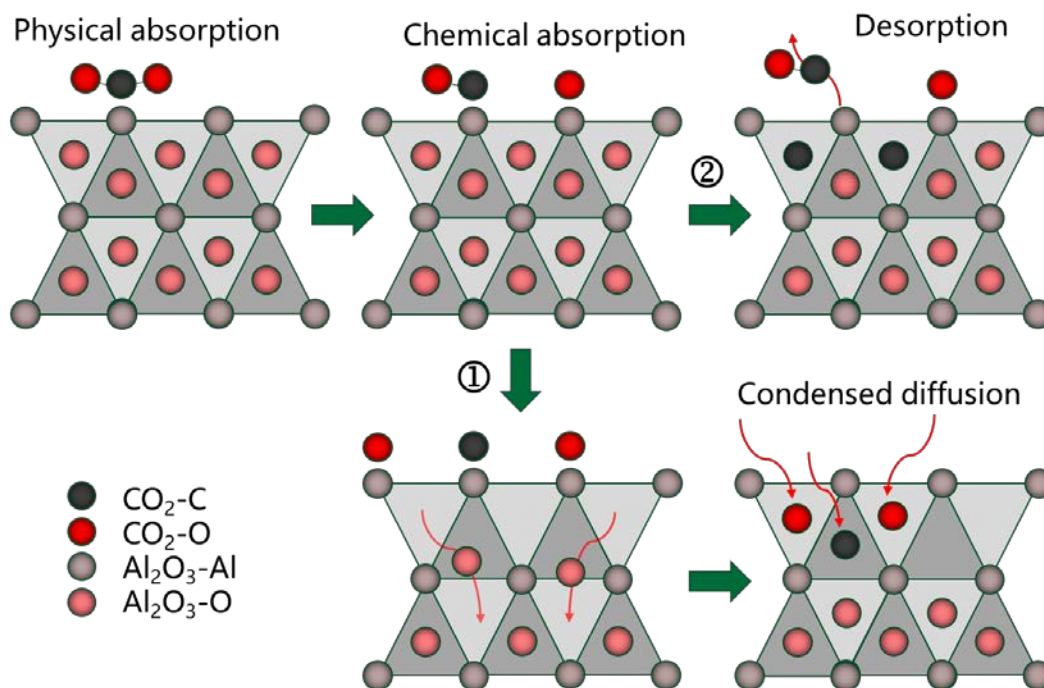
Figure 5 Schematic diagram of surface adsorption and condensed diffusion during ANP reaction.

Based on the above discussion, the reaction mechanism of ANP in CO_2 is summarized in Fig. 5. Depending on the interaction between the surface and the adsorbate, the reaction process of oxidizer and ANP is divided into three states: physical adsorption, chemical adsorption and condensed diffusion. Physical adsorption is the first step and determines the rate of the following state. Physisorption retains the chemical species of the adsorbate and the surface intact. The adsorption energy of physisorption is usually low, so that physically adsorbed molecule tends to hop on the adsorbent surface or desorption. Chemisorption involves a chemical reaction between the surface and the adsorbate, in which new chemical bonds are generated at the adsorbent surface. During the surface hopping, the oxidizer molecules might break

bond and turn into chemisorption. As the ANP temperature increases, its inner structure changes, O atoms in the oxide shell diffuse inward into core, leaving vacant sites, which helps the inward diffusion of surface adsorbed atoms. The diffusion rate of O atoms is higher than C atoms in the oxide shell, causing increase of surface C atoms and decrease of CO_2 adsorption energy (route 1). As surface C atoms concentration increases, an adsorbed CO_2 molecule is favorable to leave surface and produce CO molecule instead of diffusing into the oxide shell (route 2).

3.1.2 Heat transfer and reaction heat release

Accompanying with the oxidizer-ANP interaction, there exists heat transfer and reaction heat release. During the ANP reaction, the particle receives heat mainly from heat transfer and reaction heat release. This heating process is of vital importance to the melting and ignition of ANP. To make a quantitative analysis, the rates of heat transfer (Q_{trans}) to ANP and reaction heat release (Q_{reac}) are counted. Here the oxidizer-particle heat transfer induced by temperature difference is quantified by variation of gas kinetics energy ($dE_{KE, g}$). Since there is almost no gas phase reaction in this case (see Fig. 2a), the ANP reaction heat release can be calculated by potential energy variation of the total system ($dE_{PE, sys}$). And Q_{trans} and Q_{reac} are defined by $Q = dE/(3k_B N_p)$, where k_B is the Boltzmann constant and N_p is the number of particle atoms. The unit is K/ps, indicating the average temperature increase of each ANP atom per ps.

The temporal variations of Q_{trans} and Q_{reac} are shown in Fig. 6a. Initially, Q_{trans} is

higher, and it decreases as the ANP temperature rises. After melting, Q_{trans} turns to a negative value, indicating that the heat transfer direction is from ANP to the environment oxidizer. From the beginning, Q_{reac} increases rapidly and reaches its maximum at the ignition time. As indicated in Fig. 3b, the number of chemically adsorbed CO_2 molecules increases from the beginning of reaction, resulting in heat release from heterogeneous reaction. In Fig. 6b, Q_{trans} and Q_{reac} are integrated during each stage, to illustrate the contribution of heat transfer and reaction. It can be seen the low-temperature reaction takes place before ANP ignition, and reaction heat release plays a more important role, particularly dominating the melting and fast core oxidation stages. Besides, there is still significant reaction heat release after the Al core runs out, which comes from shell oxidation.

In conventional ANP combustion theory, the heating of the particle is mainly due to conduction and radiation heat transfer [15]. The results in this study indicate that heterogeneous surface reaction also plays an important role in particle heating before ignition. As the surface to volume ratio increases as particle radius decreases, surface reaction before ignition should be taken into consideration when modeling ANP with radius of tens of nanometers.
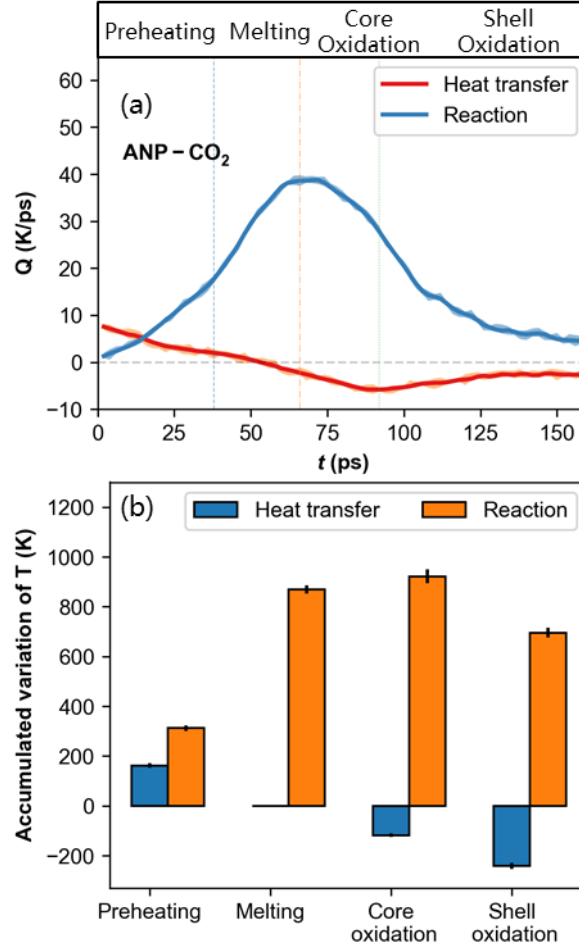
Fig. 6 Variation of heat transfer and reaction heat release rate (a) and their corresponding contribution in each stage (b).

3.2 ANP reaction in H_2O and O_2

By analyzing the trajectories of oxidizer molecules in ANP-H_2O and ANP-O_2 systems, similar processes as in ANP-CO_2 are observed. And the reaction process of ANP in hot oxidizers generally experiences physical adsorption, chemical adsorption and condensed diffusion. In the following section, the differences in the reaction process in different oxidizers and the corresponding heat/mass transfer are discussed.

3.2.1 Oxidizer-particle interaction.

Firstly, the evolutions of oxidizer molecules are compared. In the ANP-H_2O system, compared with CO_2, more radicals are observed including OH, H, O, H_2O_2. In the ANP-O_2 system, a small number of O atoms is observed. As illustrated in Fig. S2 in the supporting information, the mole fractions of radicals in both cases are less than 1% and their effect on ANP combustion can be ignored. The oxidizer molecules keep being consumed during ANP reaction except that the H_2O molecule reach saturation before ignition.

Then the numbers of oxidizer molecules indicating physisorption, chemisorption and condensed diffusion states are examined and plotted in Fig. 7. The O atom is selected to track the state of oxidizer molecules. In the ANP-H_2O system, the number of physically adsorbed molecules rapidly increases and reaches saturation near the end of preheating stage. It accelerates the preheating stage (the dash line). Then the total number of adsorbed molecules remain unchanged, however, there is a conversion from physisorption to chemisorption. After ignition, physical adsorption weakens significantly, while chemical adsorption and condensed diffusion strengthens remarkably. The reaction of ANP-O_2 is similar to ANP-CO_2, and the physical adsorption is weaker than that in the ANP-H_2O system. As illustrated in Table 1, the adsorption energy of H_2O is much lower than that of CO_2 and O_2 on the ANP surface, resulting in a higher rate of physical adsorption. In the experiments of Mohan et al. [34],

they found that ignition of Al particle in H_2O has the fastest kinetics of heterogeneous reaction. They associated the difficulty of igniting Al particles in H_2O with the relatively low heat release. Our results indicate the surface saturation may also contribute to this ignition difficulty. Before ignition, the surface reaction of ANP-CO_2 and ANP-O_2 becomes violent, and the oxidizer continuously becomes adsorbed on the ANP surface to prompt reaction. In contrast, the ANP-H_2O system experiences surface saturation, extending the melting time and furthermore causing a delay of ANP ignition.
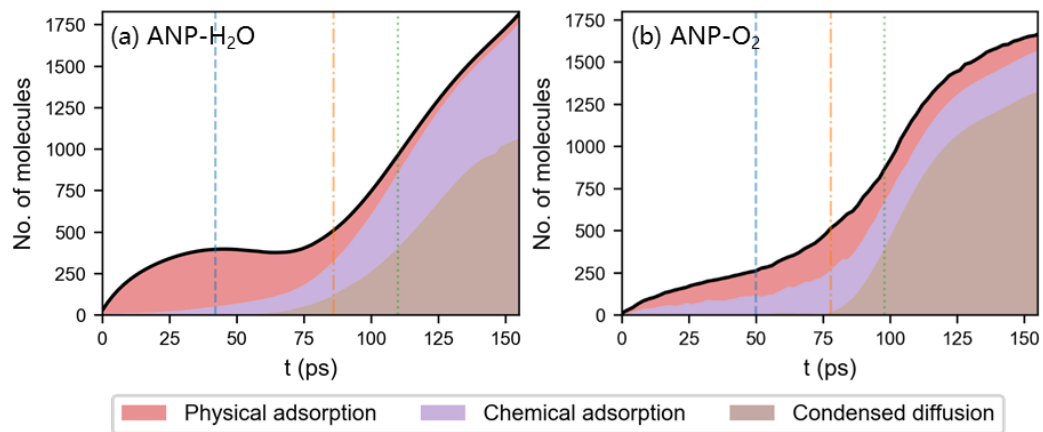

Figure 7 Temporal variations of oxidizer molecule numbers in physical, chemical adsorption and condensed diffusion states in the ANP-H_2O (a) and ANP-O_2 systems (b).

The evolutions of ANP microstructures for both cases are also examined (see Fig. S3). The inner structures of ANP are almost the same before ignition. At the end of the simulation, the atom distribution of ANP burning in O_2 is similar to that of ANP-CO_2. In the ANP-H_2O system, large amounts of H atoms diffuse into the ANP, resulting in lower oxygen atom concentration than the other two cases inside the ANP. To quantitatively analyze the atomic diffusion, the diffusivity (D) of oxidizer atoms after

ignition are calculated by the following equation [35]

$$D = \frac{1}{6N} \lim_{t \to \infty} \frac{d}{dt} \sum_{i=1}^{N} \langle [r_i(t) - r_i(0)]^2 \rangle \tag{1}$$

where N is the number of atoms, $r_i(t)$ is the position of atom i at time instant t and $r_i(0)$ is the initial position of atom i; the term $[r_i(t) - r_i(0)]$ represents the displacement of atom i after a time interval of t. The average particle temperatures from ignition to the end of simulation ($\bar{T}_p$) are also calculated, since the temperature is strongly correlated to mass diffusivity. The results are listed in Table 2.

Table 2 Mean diffusivity, particle temperature after ignition, and typical binding energy

Atom type	D (A^2/ps)	$\bar{T}_p$ (K)	Bond type	$E_{binding}$ (kcal/mol)
O in O_2	0.25141	3199.99		
O in CO_2	0.18376	2729.49	Al-O	131.231
C in CO_2	0.10488		Al-C	168.209
H in H_2O	1.94865	1947.36	Al-H	46.373
O in H_2O	0.04668			

In the three systems, the mean diffusivity of O atom in ANP increases with $\bar{T}_{ig}$, yielding a smallest value in H_2O and a highest one in O_2 system. In the ANP-CO_2 system, the diffusivity of C atoms is slower than O atoms. Thus, O atoms can diffuse inside the ANP while most C atoms remain on the outer region slightly inside the surface. In the ANP-H_2O system, the diffusivity of H atom is significantly faster than O atom. Hence, plenty of H atoms diffuse inward and most O atoms remain close to the surface. To some extent, the diffusivity of oxidizer atoms directly determines the final

ANP structure. Interestingly, in a recent ReaxFF MD simulation of ethanol/ANP combustion [18], it was found that H and O atoms can easily diffuse into ANP, but C atoms were the last to diffuse inside. CO also was observed in the latter stage of combustion. These observations are similar to the present study. It is reasonable to believe that the conclusions based on CO_2/H_2O/O_2 in this paper could be generalized to ANP reaction with hydrocarbons/alcohols which consist of C, H and O elements.

To evaluate the energy conversion during atomic diffusion, the binding energy of Al-O, Al-C and Al-H, respectively, has been analyzed by ReaxFF using a similar method as in ref. [23]. The binding energies are listed in Table 2 for Al-C, Al-O and Al-H bonds. The result shows a good agreement with that obtained by DFT and ReaxFF calculations [23,36]. For the ANP-CO_2 system, O atom has higher diffusivity than C atom in ANP, while $E_{binding}$ of O-Al is lower than that of C-Al. Similar results are found in the ANP-H_2O system. It seems that the atomic diffusivity in ANP decreases with its binding energy to Al atom, because more activation energy is needed for an atom with a higher binding energy to leave the local lattice. That is, the binding energy can directly influence the ANP structure.
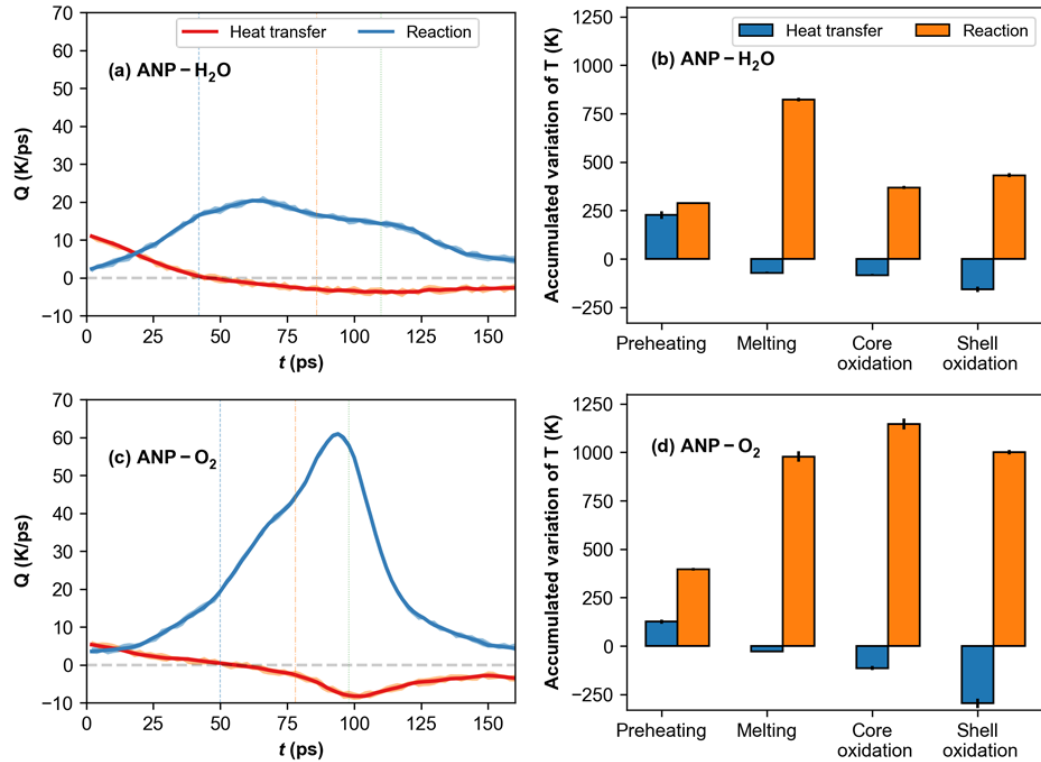
3.2.2 Heat transfer and reaction heat release

Figure 8 Variation of heat transfer and reaction heat release rate as well as their corresponding contribution in each stage in ANP reaction with H_2O (a, c) and O_2 (b, d).

The characteristics of heat transfer and reaction heat of ANP reaction in H_2O and O_2 are studied. As shown in Figs. 8a and 8c, in the ANP-H_2O system, initially Q_{trans} is high, shortening the preheating stage; Q_{reac} gradually increases to reach the peak and its peak is relatively low; for the ANP-O_2 system, Q_{reac} rapidly increases and its maximum is almost three times that of the ANP-H_2O system. Their integrated energy contributions are shown in Figs. 8b and 8d. The heat transfer of H_2O is stronger than that of O_2. Because H_2O as well as CO_2 is a triatomic molecule, which has higher kinetics energy than a diatomic molecule (O_2) under the same temperature. As a result, the energy of heat transfer in ANP-CO_2 and ANP-H_2O are higher than in ANP-O_2. In addition, the

reaction heat release in ANP-H_2O is lower because large amounts of H atoms diffuse into ANP and become bonded with Al atoms. According to the binding energies for Al-C, Al-O and Al-H, the temperature of the ANP-H_2O system is the lowest due to the low Al-H binding energy. The binding energy of Al-C is higher than that of Al-O. However, because of the poor diffusivity of C atoms, large amounts of CO molecules (around 1/3 of chemically reacted CO_2 molecules) are released to the environment, decreasing the total number of Al-C bonds. Thus, the final temperature of the ANP-CO_2 system is lower than that in ANP-O_2.
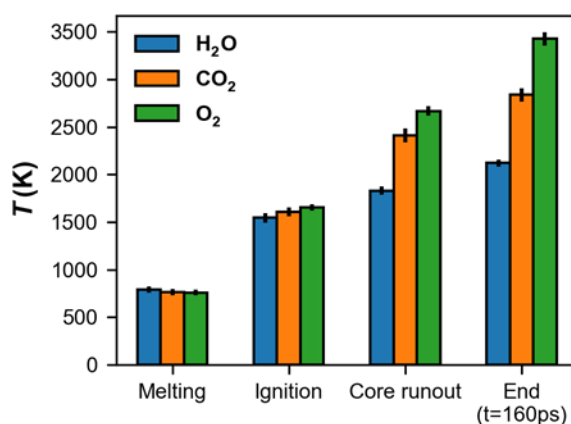

Figure 9 Particle temperature at core melting, ignition, core runout and end of simulation for ANP-CO_2, ANP-H_2O and ANP-O_2 systems.

To investigate the variation of ANP temperature during the ANP reaction with different oxidizers, particle temperatures at corresponding reaction stages are examined and plotted in Fig. 9. It is seen that the temperatures for core melting are the same in three systems, so are the ignition temperatures. Since the melting and ignition are mainly determined by the structural evolution of ANP. Before ignition, the inner structures of ANP are similar for these three systems, and the adsorbed gas molecules mostly remain on the ANP surface. However, at the instant of core runout, oxidizer

atoms diffuse inward and form different bonds with Al atoms, resulting in different ANP structures and temperatures. Plenty of Al-H bonds result in the lowest temperature at the end.

4. Conclusions

To prompt the large-scale application of aluminum nanoparticle (ANP) in propulsion systems, this study investigates the ANP reaction mechanism by systematically examining the physicochemical interactions between the ANP and the CO_2, H_2O and O_2 environments. Heat transfer and reaction heat release during the whole process are compared. Main conclusions are summarized as follows:

(1) ANP reaction generally experiences physical and chemical adsorption at the surface, and condensed diffusion inside the ANP. Before ignition, physicochemical adsorption become dominant, which prompts ANP melting via heat transfer and reaction heat release. In the ANP-H_2O reaction, owing to the low adsorption energy of H_2O, the physical adsorption is absolutely dominant at the preheating stage; for the reaction with high adsorption energy, such as ANP-O_2 and ANP-CO_2, physical adsorption becomes relatively weak and the chemical adsorption strengthens.

(2) After ignition, condensed diffusion strengthens significantly, which determines the evolution of the ANP microstructure. In this study the condensed diffusion is found to depend on the binding energy between the Al and oxidizer atoms, which

also influences the reaction heat release. With low binding energy, such as Al-H in the ANP-H_2O system, the oxidizer atoms (e.g., H atom) are prone to diffuse into the ANP, yielding low reaction heat release. In contrast, the high-binding-energy atoms (e.g., Al-C in ANP-CO_2) show weak diffusivity in the ANP, and only limited Al-C bonds are formed owing to desorption of CO, yielding lower heat release than the ANP-O_2 system.

(3) The inner structures of ANPs are not affected by the oxidizer before ignition. As a result, the temperatures for Al core melting and ANP ignition are almost the same for different oxidizer types. Reaction heat release is more significant than heat transfer for ANP melting and ignition.

Through revealing the detailed interaction processes between the ANP and the environmental oxidizer, this study gains insight into the heterogeneous and condensed phase reaction of aluminum nanoparticles. It also suggests methods to improve control of ANP reaction by manipulating physicochemical adsorption and condensed diffusion at different stages, for example, via adjusting oxidizer properties.

Supporting Information

The sensitivities of bin selection for the surface region (Fig. S1); the evolution of ambient molecules and ANP structure for ANP-H_2O and ANP-O_2 system (Fig. S2-3).

Author information

Corresponding authors:

Baolu Shi (shibaolu@bit.edu.cn)   ORCID: 0000-0002-8638-4679

Lijuan Liao (liaohuanxin@hotmail.com)   ORCID: 0000-0003-1753-6373

Acknowledgment

Reference

[1]   T.R. Sippel, T.L. Pourpoint, S.F. Son, Combustion of nanoaluminum and water propellants: Effect of equivalence ratio and safety/aging characterization, Propellants, Explos. Pyrotech. 38 (2013) 56–66. doi:10.1002/prep.201200143.

[2]   H.T. Huang, M.S. Zou, X.Y. Guo, R.J. Yang, Y.K. Li, Analysis of the aluminum reaction efficiency in a hydro-reactive fuel propellant used for a water ramjet, Combust. Explos. Shock Waves. 49 (2013) 541–547. doi:10.1134/s0010508213050055.

[3]   J.M. Bergthorson, Y. Yavor, J. Palecka, W. Georges, M. Soo, J. Vickery, S. Goroshin, D.L. Frost, A.J. Higgins, Metal-water combustion for clean propulsion and power generation, Appl. Energy. 186 (2017) 13–27. doi:10.1016/j.apenergy.2016.10.033.

[4]   P. Bucher, R.A. Yetter, F.L. Dryer, E.P. Vicenzi, T.P. Parr, D.M. Hanson-Parr, Condensed-phase species distributions about Al particles reacting in various oxidizers, Combust. Flame. 117 (1999) 351–361. doi:10.1016/S0010-2180(98)00074-1.

[5]   Y.S. Kwon, A.A. Gromov, A.P. Ilyin, E.M. Popenko, G.H. Rim, The mechanism of combustion of superfine aluminum powders, Combust. Flame. 133 (2003) 385–391. doi:10.1016/S0010-2180(03)00024-5.

[6]   J. Prentice, Combustion of laser-ignited aluminum droplets in wet and dry

        oxidizers, in: 12th Aerosp. Sci. Meet., 1974: p. 146.

[7]   T.A. Roberts, R.L. Burton, H. Krier, Ignition and combustion of

        aluminummagnesium alloy particles in O2 at high pressures, Combust. Flame.

        92 (1993) 125–143.

[8]   E.L. Dreizin, On the mechanism of asymmetric aluminum particle combustion,

        Combust. Flame. 117 (1999) 841–850.

[9]   E.L. Dreizin, Experimental study of aluminum particle flame evolution in

        normal and micro-gravity, Combust. Flame. 116 (1999) 323–333.

[10]   K. Brandstadt, D.L. Frost, J.A. Kozinski, Preignition characteristics of nano-

        And micrometer-scale aluminum particles in Al-CO2 oxidation systems, Proc.

        Combust. Inst. 32 II (2009) 1913–1919. doi:10.1016/j.proci.2008.08.014.

[11]   V.I. Levitas, K. Samani, Size and mechanics effects in surface-induced melting

        of nanoparticles, Nat. Commun. 2 (2011) 284–286. doi:10.1038/ncomms1275.

[12]   P. Lynch, H. Krier, N. Glumac, A correlation for burn time of aluminum

        particles in the transition regime, Proc. Combust. Inst. 32 II (2009) 1887–1893.

        doi:10.1016/j.proci.2008.06.205.

[13]   T. Bazyn, H. Krier, N. Glumac, Combustion of nanoaluminum at elevated

        pressure and temperature behind reflected shock waves, Combust. Flame. 145

(2006) 703–713.

[14] N. Glumac, H. Krier, T.I.M. Bazyn, R. Eyer, Temperature measurements of aluminum particles burning in carbon dioxide, Combust. Sci. Technol. 177 (2005) 485–511.

[15] D.S. Sundaram, P. Puri, V. Yang, A general theory of ignition and combustion of nano- and micron-sized aluminum particles, Combust. Flame. 169 (2016) 94–109. doi:10.1016/j.combustflame.2016.04.005.

[16] M.W. Beckstead, Correlating Aluminum Burning Times, Combust. Explos. Shock Waves. 41 (2005) 533–546. doi:10.1007/s10573-005-0067-2.

[17] H.D. Zeng, X.L. Cheng, C.Y. Zhang, Z.P. Lu, Responses of Core-Shell Al/Al2O3 Nanoparticles to Heating: ReaxFF Molecular Dynamics Simulations, J. Phys. Chem. C. 122 (2018) 9191–9197. doi:10.1021/acs.jpcc.8b01088.

[18] Y.R. Zhang, A.C.T. van Duin, K.H. Luo, Investigation of ethanol oxidation over aluminum nanoparticle using ReaxFF molecular dynamics simulation, Fuel. 234 (2018) 94–100. doi:10.1016/j.fuel.2018.06.119.

[19] B.J. Henz, T. Hawa, M.R. Zachariah, On the role of built-in electric fields on the ignition of oxide coated nanoaluminum: Ion mobility versus fickian diffusion, J. Appl. Phys. 107 (2010). doi:10.1063/1.3247579.

[20] W. Wang, R. Clark, A. Nakano, R.K. Kalia, P. Vashishta, Fast reaction

mechanism of a core(Al)-shell (Al2O3) nanoparticle in oxygen, Appl. Phys. Lett. 95 (2009) 1–4. doi:10.1063/1.3268436.

[21]   Q. Chu, B. Shi, L. Liao, K.H. Luo, N. Wang, C. Huang, Ignition and Oxidation of Core-Shell Al/Al 2 O 3 Nanoparticles in an Oxygen Atmosphere: Insights from Molecular Dynamics Simulation, J. Phys. Chem. C. 122 (2018) 29620–29627. doi:10.1021/acs.jpcc.8b09858.

[22]   S. Hong, A.C.T. Van Duin, Molecular Dynamics Simulations of the Oxidation of Aluminum Nanoparticles using the ReaxFF Reactive Force Field, J. Phys. Chem. C. 119 (2015) 17876–17886. doi:10.1021/acs.jpcc.5b04650.

[23]   S. Hong, A.C.T. Van Duin, Atomistic-scale analysis of carbon coating and its effect on the oxidation of aluminum nanoparticles by ReaxFF-molecular dynamics simulations, J. Phys. Chem. C. 120 (2016) 9464–9474. doi:10.1021/acs.jpcc.6b00786.

[24]   P. Liu, J. Liu, M. Wang, Ignition and combustion of nano-sized aluminum particles: A reactive molecular dynamics study, Combust. Flame. 201 (2019) 276–289. doi:10.1016/j.combustflame.2018.12.033.

[25]   X. Zhang, C. Fu, Y. Xia, Y. Duan, Y. Li, Z. Wang, Y. Jiang, H. Li, Atomistic Origin of the Complex Morphological Evolution of Aluminum Nanoparticles during Oxidation: A Chain-like Oxide Nucleation and Growth Mechanism, ACS Nano. 13 (2019) 3005–3014. doi:10.1021/acsnano.8b07633.

[26] H. Zeng, X. Cheng, C. Zhang, Z. Lu, Responses of Core–Shell Al/Al 2 O 3 Nanoparticles to Heating: ReaxFF Molecular Dynamics Simulations, J. Phys. Chem. C. 122 (2018) 9191–9197. doi:10.1021/acs.jpcc.8b01088.

[27] Y. Jiang, S. Deng, S. Hong, J. Zhao, S. Huang, C.C. Wu, J.L. Gottfried, K.I. Nomura, Y. Li, S. Tiwari, R.K. Kalia, P. Vashishta, A. Nakano, X. Zheng, Energetic Performance of Optically Activated Aluminum/Graphene Oxide Composites, ACS Nano. 12 (2018) 11366–11375. doi:10.1021/acsnano.8b06217.

[28] P. Liu, R. Sun, J. Liu, Adsorption behaviors of ether and aluminum surface: A molecular dynamics study, Int. J. Mod. Phys. B. 33 (2019) 1950028. doi:10.1142/s0217979219500280.

[29] S. Plimpton, Fast parallel algorithms for short-range molecular dynamics, J. Comput. Phys. 117 (1995) 1–19. doi:10.1006/jcph.1995.1039.

[30] A. Stukowski, Visualization and analysis of atomistic simulation data with OVITO-the Open Visualization Tool, Model. Simul. Mater. Sci. Eng. 18 (2010). doi:10.1088/0965-0393/18/1/015012.

[31] P. Heitjans, J. Kärger, Diffusion in condensed matter: methods, materials, models, Springer Science & Business Media, 2006.

[32] X. Wang, C. Bu, J. Zhang, D. Chen, H. Xie, G. Piao, Adsorption of Lead ,

Cadmium , Sodium and Potassium Vapor Molecular on Met a-kaolinite

Surface : A DFT Study Modeling and Computational Details, (2019) 1–5.

[33]   Z. Wang, J. Liu, B. Zhang, Y. Yang, Z. Zhang, S. Miao, Mechanism of

Heterogeneous Mercury Oxidation by HBr over V2O5/TiO2 Catalyst, Environ.

Sci. Technol. 50 (2016) 5398–5404. doi:10.1021/acs.est.6b00549.

[34]   S. Mohan, L. Furet, E.L. Dreizin, Aluminum particle ignition in different

oxidizing environments, Combust. Flame. 157 (2010) 1356–1363.

doi:10.1016/j.combustflame.2009.11.010.

[35]   J. Desbrières, V.G. Babak, Interfacial properties of amphiphilic natural, Polym.

55 (2006) 1177–1183. doi:10.1002/pi.

[36]   P. Liu, J. Liu, M. Wang, Adsorption of ethanol molecules on the Al (1 1 1)

surface: a molecular dynamic study, R. Soc. Open Sci. 6 (2019) 181189.

doi:10.1098/rsos.181189.